Water Air Soil Pollut (2026) 237:593
https://doi.org/10.1007/s11270-026-09282-x

Valorization of Foundry Waste into Iron-Based Coagulant and Ceramic Additives

Volha Zalyhina · Valentin Romanovski

Received: 21 June 2025 / Accepted: 12 February 2026

Abstract Wastewater purification from suspended and colloidal impurities remains a critical challenge for industrial and municipal water management. This study proposes a sustainable iron-based coagulant synthesized from foundry waste, enabling simultaneous wastewater treatment and industrial waste recycling. The magnetic fraction of foundry dust (Fe ≈ 47.7 wt%) was leached with HCl to produce an iron-containing coagulant, while the non-magnetic fraction was evaluated for ceramic applications. The obtained coagulant demonstrated high purification performance at an optimal dose of 37.5 mg/L, achieving > 95% removal of suspended solids within pH 5–7 across three types of model wastewater (clay 5 g/L, glaze 10 g/L, dairy 40 mL/L). Compared to commercial $FeCl_3$, the experimental coagulant required up to 6–12 times lower dose to reach 97–98% clarification efficiency. This effect is attributed to the simultaneous presence of iron species and polysilicic flocculants formed during waste acid treatment. Additionally, leaching residues and the non-magnetic fraction were successfully incorporated (10–30 wt%) into artistic ceramics without compromising density or water absorption. The proposed approach demonstrates a dual environmental benefit – valorization of iron-rich industrial waste and reduced chemical consumption during coagulation – contributing to SDG 6 (Clean Water and Sanitation) and SDG 12 (Responsible Consumption and Production).

Keywords Coagulation · Iron coagulant · Wastewater treatment · Foundry waste · Sustainable development

1 Introduction

Water plays an extremely important role in human life. Only fresh water is used for industrial and domestic needs of mankind, making up about 3% of its total reserves. When water is used, it becomes contaminated with substances of mineral (Martsul et al., 2013; Zalyhina et al., 2021) and organic origin (Gurgenidze & Romanovski, 2023; Matsukevich et al., 2025; Romanovski et al., 2025), which leads to the formation of a large amount of wastewater. Most wastewater is contaminated with suspended matter and is a dispersed system, which, according to the degree of particle dispersion, is divided into suspensions and emulsions with a particle diameter of more than 10^{-5} cm and colloidal solutions with a particle diameter of 10^{-5} to 10^{-7} cm. Many natural and wastewaters are colloidal systems, which are extremely difficult to purify due to their stability. Among

V. Zalyhina
Belarusian State Technological University, Sverdlova, 13a, 220006 Minsk, Belarus

V. Romanovski (✉)
Department of Materials Science and Engineering, University of Virginia, Charlottesville, VA 22904, USA
e-mail: rvd9ar@virginia.edu

Published online: 23 February 2026

different filtering approaches (Gudkov et al., 2021, 2022) coagulants and flocculants are used to disrupt the stability of dispersed systems, which have found wide application in the practice of purifying natural water and wastewater (Prakash et al., 2014; Richardson & Connelly, 2018). The most commonly used coagulants are aluminum and iron salts: iron sulfate $FeSO_4$, aluminum sulfate $Al_2(SO_4)_3$, iron (III) chloride ($FeCl_3$), aluminum hydroxysulfate ($Al(OH)SO_4$), etc. (Gruzinova & Romanovski, 2025).

The recycling of waste to obtain valuable substances and materials (Bratchun et al., 2024; Brigida et al., 2024; Klyuev et al., 2024; Ma et al., 2024; Malyukova et al., 2023; Vafaeva et al., 2024; Yelaman et al., 2025) is a relevant area and complies with SDG 12 (Beletskii & Romanovski, 2024; Kamarou et al., 2025; Kozlovskaya et al., 2024; Romanovski et al., 2024). Of particular relevance is the development of materials for water purification (Romanovskiy, 2011). Currently, the need for coagulants is constantly growing, and the raw material base for their production is limited. Therefore, it is very important to obtain coagulants from production waste, which, in this case, can be considered a secondary material resource. Processing waste to obtain coagulants will also solve the environmental problem (pollution of the environment with waste) and get closer to waste-free technologies.

One of the industries where iron-containing waste is formed, which can be used to obtain coagulants, is foundry production. The foundry process includes three stages: melting the metal, making casting molds, and obtaining castings. Making casting molds includes preparing the molding and core mixture, making half-molds and cores, and assembling the casting molds. A casting mold is a system of elements that form a working cavity, which is filled with alloy to form a casting. After cooling and hardening, the castings are knocked out of the molds, cleaned, and, if necessary, subjected to additional heat treatment. Three types of waste are generated in the foundry industry: burnt molding earth, metallurgical slag, and iron-containing dust. Iron-containing dust is generated during the cleaning of the casting surface in various ways: in periodic and continuous drums, in shot blasting drums, on shot blasting tables, in shot blasting chambers, etc. Iron-containing dust contains up to 25% iron.

Currently, there are quite a lot of developments in the processing of metallurgical slags and molding burnt earth (Zalyhina et al., 2022). Much less attention is paid to the issues of processing iron-containing dust, possibly due to the smaller amount of its formation compared to other wastes of the foundry industry. Meanwhile, given the high iron content in it, it is a valuable secondary material resource that can find application in various industries, in particular, for the production of iron-containing coagulants. Many works are devoted to the production of coagulants, including the regeneration of coagulants from coagulation sediments (Blel et al., 2015; Stevenson et al., 1933). Among the wastes used to obtain coagulants, red mud, mining wastes, iron-containing solutions, etc., were considered. Technologies for processing mineral waste, such as bauxite, are also aimed at extracting aluminum sulfates from them (Couperthwaite et al., 2013). Waste from the processing of ferrous and non-ferrous metals, including slag and dust, is often used to obtain iron chlorides (Matei et al., 2022). For example, in the study (Owodunni & Ismail, 2021), an iron-based coagulant was developed from vegetable oil production waste. Also, in the work (Tuzhilin et al., 2020), the production of basic aluminum chloride from aluminum hydroxide formed during the etching of aluminum products is described. In the study (Lal & Garg, 2019), an aluminum-based coagulant was synthesized from paper industry waste, which demonstrated high efficiency in removing suspended solids. Another example is the production of a mixed coagulant from iron ore tailings (Almeida & Schneider, 2020), where acid leaching was used to extract iron and aluminum in the form of sulfates. In recent years, methods for obtaining coagulants from industrial waste have been actively studied, which contributes to the environmental safety and economic efficiency of water purification processes. For example, iron-containing coagulants are obtained from spent pickling solutions of steel rolling plants containing sulfates and iron (II) chlorides by oxidizing iron (II) to iron (III) using sodium hypochlorite (Peters et al., 1987). Similarly, mixed coagulants are obtained from iron ore beneficiation waste that is rich in iron oxides by leaching with sulfuric acid at elevated temperatures (Mwewa et al., 2019). Also, aluminum sulfate, used as a coagulant, is obtained from aluminum production waste, such as alumina slag, by leaching with sulfuric acid (Orescanin et al., 2002;

Poulin et al., 2008; Zhao et al., 2011). These methods allow for the efficient utilization of industrial waste and the production of coagulants that facilitate effective water purification.

Although recent studies have successfully explored waste-derived coagulants synthesized from red mud, acid mine drainage, steel pickling liquors and industrial effluents, several important shortcomings remain. For example, red-mud-based coagulants often require multi-stage precipitation and neutralization steps (Orescanin et al., 2002; Poulin et al., 2008; Zhao et al., 2011), while poly-aluminoferric coagulants obtained from acid mine drainage demand additional chemical oxidation and pH adjustment (Mwewa et al., 2019). Coagulants derived from spent pickling liquors rely on hypochlorite oxidation and generate secondary chloride-rich effluents (Peters et al., 1987). Iron-based coagulants produced from iron ore tailings or industrial residues (Almeida & Schneider, 2020; Matei et al., 2022) demonstrate promising performance, but typically require high reagent consumption or deliver removal efficiencies below those of commercial $FeCl_3$/$Al_2(SO_4)_3$ standards. Importantly, most recent studies focus exclusively on coagulant synthesis and neglect downstream utilization of solid residues, which limits the circularity and techno-economic viability of these routes. Notably, iron-containing foundry dust, despite containing up to 40–50 wt% iron and being continuously generated in casting operations, remains poorly investigated as a feedstock for coagulant production (Zalyhina et al., 2022, 2024). Therefore, introducing a process that (a) valorizes foundry dust into a functional iron-based coagulant, (b) matches or exceeds commercial performance at significantly lower dosages, and (c) enables beneficial reuse of the non-magnetic fraction in ceramic products represents a clear technological novelty and contribution to sustainable materials engineering.

Despite the wide availability of commercial aluminum- and iron-based coagulants, their production relies on primary mineral resources and generates significant amounts of process waste, which limits their sustainability and economic feasibility in regions without strong raw material bases. At the same time, large quantities of iron-rich residues are continuously generated in metal processing, casting and surface finishing industries, yet their utilization remains limited primarily to low-value landfill disposal or partial recycling. This mismatch between (i) increasing demand for cost-effective coagulants, (ii) restricted raw material availability, and (iii) underutilized iron-bearing waste streams defines a clear technological gap. Recent studies have explored red mud, mining residues and industrial effluents as feedstock for coagulant synthesis, but foundry iron-containing dust remains largely uninvestigated, despite containing up to 40–50 wt% iron and being widely available in casting facilities. Therefore, a systematic assessment of foundry waste valorization into functional water treatment coagulants is both environmentally and economically justified. The present work addresses this gap by synthesizing an iron-based coagulant from foundry dust, evaluating its coagulation efficiency against commercial analogues across different wastewater types, and assessing the utilization potential of the non-magnetic fraction in ceramic materials.

The objectives of this work were:

i) to obtain an iron-containing coagulant from foundry waste; *ii*) to study the coagulating properties of the obtained material and determine its efficiency in comparison with a commercial coagulant; *iii*) to evaluate the effect of pH and coagulant dose on the efficiency of wastewater treatment; and *iv*) to evaluate the possibility of using the non-magnetic fraction in the production of ceramic products.

2 Materials and Methods

2.1 Materials and Reagents

Iron-containing dust (ICD) obtained from foundry production was used as the raw material for coagulant synthesis. Hydrochloric acid of chemically pure grade (GOST 3118–77, Russia) was used as the leaching reagent. A commercial ferric chloride coagulant ($FeCl_3 \cdot 6H_2O$, Belhim) was used as the reference. Clay and glaze powders with particle sizes below 50 µm were used to prepare wastewater samples. Studies to determine the purification efficiency using the obtained experimental coagulant were conducted on three model wastewaters: *i*) model wastewater WW1 from ceramic production, contaminated with fine clay impurities (5 g/L); *ii*) model wastewater WW2 from glaze production, contaminated with fine glaze powder impurities (10 g/L); *iii*) model wastewater WW3

from a fermented milk production facility, contaminated with yogurt impurities (40 mL/L). Before use, the resulting coagulant solution was diluted to a 3% concentration.

2.2 Samples Synthesis

The synthesis of the iron-based coagulant was performed using the magnetic fraction of iron-containing dust (ICD) obtained after magnetic separation. In a typical procedure, 5.00 g of magnetic ICD were weighed (analytical balance, ± 0.001 g) and transferred into a 250 mL glass reactor equipped with a mechanical stirrer and a reflux condenser. Hydrochloric acid solution (18 wt%) was prepared by dilution of concentrated HCl (37 wt%, 12 M, Merck) with deionized water to the required concentration; the final molarity of the working HCl solution was approximately 6.0 M. The acid was added to the reactor in a solid-to-liquid ratio of 1:7, corresponding to 35 mL of 18 wt% HCl per 5.00 g of ICD.

After the addition of the acid, the suspension was stirred and heated to 100 °C using an water bath, and maintained at this temperature for 30 min. The reaction was accompanied by noticeable hydrogen evolution due to the dissolution of metallic iron. Upon completion of the heating stage, the reactor was removed from the bath and left under continuous stirring at room temperature (22–25 °C) for 12 h to ensure complete iron leaching and oxidation of Fe^{2+} species. After the holding stage, the suspension was vacuum-filtered through a 0.45 μm cellulose nitrate membrane. The filtrate (liquid phase) represented the iron-containing coagulant solution, while the solid residue (leaching sludge) was washed three times with 50 mL portions of deionized water and dried at 100 °C for 4 h for further characterization.

The final iron-containing coagulant solution had a total Fe concentration of approximately 70 g/L, determined according to Sect. 2.4. Prior to use in coagulation tests, the stock solution was diluted to 3 wt% Fe by deionized water. All synthesis steps were performed in triplicate to verify reproducibility.

2.3 Wastewater Treatment Experiment

To determine the optimal dose, five coagulant dosages were tested corresponding to 0, 12.5, 25.0, 37.5 and 50.0 mg of dry coagulant per liter of wastewater (mg/L). For each experiment, 40 mL of model wastewater were placed into glass cylinders, and the required volume of the coagulant solution was added using a micropipette to achieve the specified dose. After mixing the coagulant, the purified water was settled for 15 min. During the settling process, visual observation of the process of formation of aggregates and their sedimentation was carried out. After 15 min, samples of purified water were taken, and their turbidity (by optical density) was determined. The studies were carried out at different pH values (5, 6, 7), which were adjusted using a 1 M KOH solution.

The efficiency of water purification Ef (%) was calculated using the Eq. (1):

$$Ef = \frac{D_0 - D}{D_0} \bullet 100\% \quad (1)$$

where D_0 – optical density of contaminated water, D – optical density of purified water.

Based on the calculated cleaning efficiency, the optimal dose of coagulant was determined.

2.4 Samples Analysis

X-ray phase analysis was performed using a D8 Advance diffractometer (Bruker AXS, Germany). The analysis was made in the direction of the angle 2θ 10–80° with a step of 0.1–0.2° and accumulation of pulses for 2 s. Identification of the obtained X-ray patterns was carried out using specialized HighScore Plus software and the PDF-2 database.

The structure and elemental composition were determined by electron microscopic analysis on a JSM-5610 LV scanning electron microscope with an EDX JED-2201 electron probe energy-dispersive chemical analysis system (JEOL, Japan).

The amount of hygroscopic moisture was determined according to GOST 23581.1–79 'Iron ores, concentrates, and agglomerates'. The sample is placed in a weighing bottle, pre-dried at 105 ± 2 °C until the mass is constant and weighed, and dried in a drying cabinet at 105 ± 2 °C for 1 h; then the lid of the weighing bottle is closed, cooled in a desiccator for 20–25 min, and weighed. Before weighing, slightly open the lid of the weighing bottle and then quickly close it. Drying is repeated for 25–30 min until a constant mass is obtained. The mass fraction

of hygroscopic moisture X (%) was calculated using the Eq. (2):

$$W_h = \left(m_1 - m_2\right)100/m \quad (2)$$

where m_1 is the mass of the sample with the crucible before drying, g; m_2 is the mass of the sample with the crucible after drying, g; m is the mass of the sample before drying, g.

The mass loss on ignition of the obtained samples was determined by GOST 2642.2–86 "Refractory Materials and Products". A 0.5–1.0 g sample of ore, concentrate, agglomerate, or pellets was placed in a porcelain crucible, calcined at 900 °C, weighed, placed in an even layer, and calcined in a muffle furnace. The temperature in the furnace was gradually increased to 900–1000 °C, and the sample was calcined at this temperature for 2 h. After cooling in a desiccator, the crucible with the sample was weighed. The mass loss on ignition X_{mli} (%) was determined by the Eq. (3):

$$X_{mli} = \left(\left(m_1 - m_2\right)100/m - W_h\right)K, \quad (3)$$

where m_1 is the mass of the sample with the crucible before calcination, g; m_2 is the mass of the sample with the crucible after calcination, g; m is the mass of the sample before calcination, g; W_h is the mass fraction of hygroscopic moisture in the analyzed sample, %; K is the conversion factor for the loss of mass on calcination in dry material, calculated using the Eq. (4).

$$K = 100/\left(100 - W_h\right) \quad (4)$$

The mass fraction of iron in the mixture (X) is determined by GOST 25216–82 "Method for Determining Iron". A 20 g sample of iron-containing dust is spread in an even layer no more than 3 mm thick on a sheet of clean paper or dry, clean glass. The magnet is wrapped in a piece of paper, and the poles of the magnet are slowly moved along the surface of the scattered material, moving it sequentially in two mutually perpendicular directions so that the entire sample is covered by the magnetic field. Then the magnet is transferred to a sheet of clean paper, the paper covering it is unfolded, and the magnetic particles are sprinkled. The extraction of magnetic particles is repeated three times. Before each extraction, the sample is thoroughly mixed and spread in an even layer no more than 3 mm thick. If there are iron particles in the obtained material, a control extraction of magnetic particles is carried out, while the poles of the magnet should be removed from the surface of the material at a distance of 5–10 mm. The extracted magnetic particles are weighed, Eq. (5).

$$X = m100/m_1 \quad (5)$$

where m is the mass of iron extracted by the magnet, g; m_1 is the mass of the sample.

The concentration of Fe (II, III) ions was determined by the photocolorimetric method with sulfosalicylic acid; the range of measured concentrations was $0.1-10$ mg/L [9]. The determination is based on the formation of colored complexes of Fe (II, III) ions with sulfosalicylic acid. In a slightly acidic medium ($pH>4$), sulfosalicylic acid interacts only with Fe (III) ions, forming a red complex stable at pH 4–8. In an alkaline medium (pH 8–11.5), sulfosalicylic acid reacts with Fe (III) and Fe (II) ions, forming a yellow complex. The Fe (II) content was found by the difference in the content of total iron and Fe (III). The optical density of the analyzed solutions was measured at a wavelength of $\lambda=425$ nm for total iron and at a wavelength of λ 500 nm for Fe (III). The relative measurement error for the range of $1.0-5.0$ mg/L was $\pm 15\%$, for the range of $5.0-10$ mg/L $\pm 10\%$. If the concentration of Fe (II, III) ions in the analyzed sample exceeded 10 mg/L, it was diluted so that the concentration of iron ions corresponded to the regulated range.

pH was measured using an I-160 M pH meter equipped with a combined glass electrode ESKL-08. M1, measurement range $0-12$, measurement accuracy ± 0.2 pH units.

Three parallel experiments were carried out to determine all properties, after which the average value was calculated.

2.5 Use of Leaching Sludge and Non-Magnetic Fraction of Liquid-Coal-Bearing Minerals in the Production of Artistic Ceramics

Experimental ceramic samples were made from clay from the Gaidukovsky deposit (Belarus) with the addition of waste from 10 to 30 wt.%. The molding was carried out by hand molding with subsequent

drying at 100 ºC and firing at a temperature of 1000 ºC.

The bulk density (ρ, g/cm^3) of the sintered ceramic samples was determined according to the Archimedes method. Samples were weighed in dry state (m_1), saturated in water under vacuum for 2 h and subsequently weighed in saturated state (m_2) and in water (m_3). The density was calculated as, Eq. (6):

$$\rho = m_1/(m_2 - m_3) \quad (6)$$

Water absorption (WA, wt.%) was measured according to the standard procedure used for ceramic materials. After oven drying at 105 °C (24 h), specimens were weighed (m_{dry}), immersed in water for 24 h, surface dried and weighed (m_{wet}). Water absorption was calculated as, Eq. (7):

$$WA = \left[(m_{wet} - m_{dry})/m_{dry}\right]100\% \quad (7)$$

These methods are widely applied for assessing ceramic products and correspond to ISO 10545–3(2018) and ASTM C373-18 procedures.

3 Results and Discussions

3.1 Analysis of Iron-Containing Dust

In this study, the waste material was characterized in terms of hygroscopic moisture content, loss on ignition, iron content, and both elemental and phase composition. The waste moisture content was 2.44%, and the loss on ignition was 0.47%. X-ray phase analysis (Fig. 1) indicates that the main crystalline phase of the ICD is quartz sand (SiO_2). SiO_2 is presented in the form of quartz phases with a hexagonal crystal system and P3221 space group, as well as a cristobalite with a tetragonal crystal system and P41212 space group. Iron is presented in the form of hematite phase Fe_2O_3 with a cubic crystal system and Fd-3 m space group and metallic iron with a cubic crystal system and Im-3 m space group.

XRD was used exclusively to identify crystalline phases and does not provide elemental composition (Fig. 1, Fig. 2). Therefore, the elemental composition of the initial ICD and its magnetic and non-magnetic fractions was evaluated by SEM–EDS. SEM–EDS analysis provides

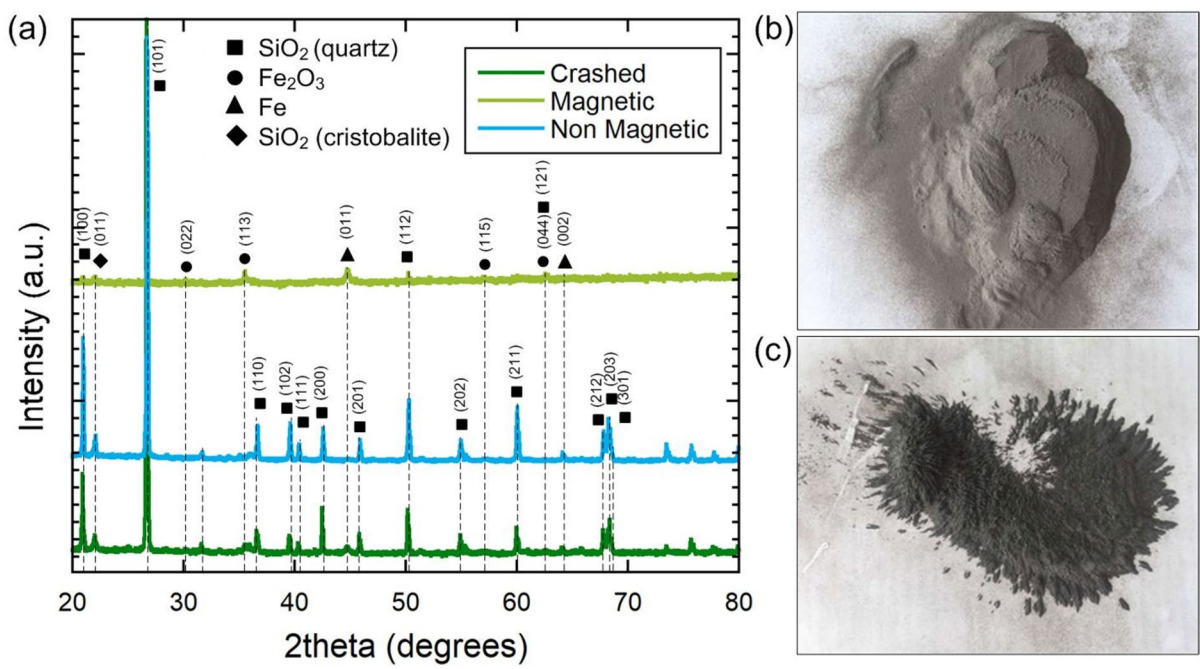

Fig. 1 XRD patterns of the original iron-containing dust and its separated fractions **a**, and optical images of the non-magnetic **b** and magnetic **c** fractions

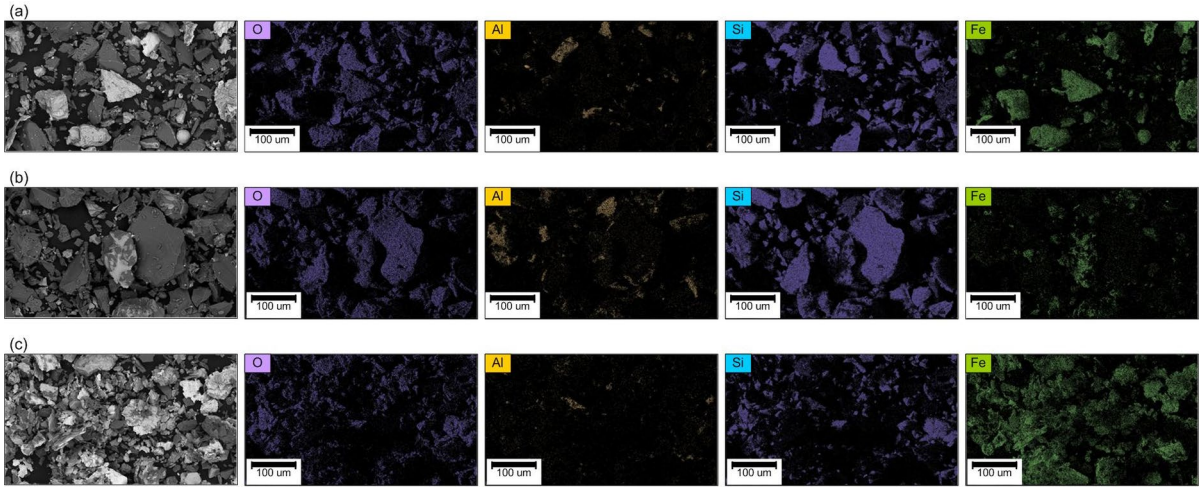

Fig. 2 SEM–EDS images of the crushed iron-containing dust **a**, non-magnetic fraction **b** and magnetic fraction **c**

Table 1 Elemental composition of the iron-containing dust and its fractions determined by SEM–EDS, wt%

Element	ICD, wt.%	Magnetic fraction, wt.%	Non-magnetic fraction, wt.%
O	50.17	32.27	53.03
Si	40.06	18.27	43.42
Fe	8.27	47.79	2.03
Al	1.50	1.31	1.52

semi-quantitative elemental composition, and the reported mass percentages in Table 1 correspond to normalized EDS values generated by the instrument's quantification software (ZAF correction, averaged over $N \geq 5$ measurement points). These values are intended to indicate relative enrichment and depletion of specific elements between fractions. The absolute iron content (52 wt% for ICD and 47.7 wt% for the magnetic fraction) was later determined independently by magnetic separation and gravimetric weighing in accordance with GOST 25216–82 (see Sect. 2.4), and therefore does not rely on EDS data. Table 1 shows that after magnetic separation, the iron content in the magnetic component, compared to iron-containing dust, increased almost 6 times and amounted to 47.70 wt.%.

The high iron content in the magnetic fraction confirms the possibility of using this waste to produce iron-containing coagulant. The verification was based on the elemental analysis of the magnetic fraction, which showed an Fe content of 47.7 wt% (Table 1), determined by SEM–EDS and confirmed by gravimetric magnetic separation in accordance with GOST 25216–82. Such iron content is sufficient for subsequent acid leaching to produce Fe^{2+}/Fe^{3+} salts in aqueous solution, which are the active species in iron-based coagulants (e.g., $FeCl_3$ or hydrolyzed Fe^{3+} complexes). Therefore, the high Fe concentration in the magnetic fraction confirms its suitability as a feedstock for coagulant synthesis. Iron-containing foundry dust typically contains a significant silica fraction originating from the breakup of molding sand and core materials used in casting operations. Most foundry molding sands consist predominantly of quartz ($SiO_2 > 95$ wt.%), while auxiliary refractories and core binders contain additional silica and aluminosilicate phases. During pouring, shake-out and shot blasting, fine quartz particles become airborne and accumulate in the dust collection system. This explains the presence of SiO_2 detected in the non-magnetic fraction of ICD. From a compositional standpoint, the ICD investigated in this study is characterized by a relatively high bulk iron content (52 wt.%) and a magnetically enriched fraction containing 47.7 wt.% Fe, while the non-magnetic fraction is dominated by quartz and cristobalite with only minor alumina and very low loss on ignition (0.47 wt.%). This bimodal Fe–SiO_2 character is consistent with reported data for iron-rich

foundry dusts and spent molding sands, where silica is the major mineral phase and iron contents typically range between 20 and 50 wt.% (Matei et al., 2022; Zalyhina et al., 2022). Compared with other iron-bearing residues used for coagulant synthesis, such as red mud, alumina slags or iron ore tailings (Almeida & Schneider, 2020; Matei et al., 2022; Poulin et al., 2008), the ICD shows a higher proportion of readily magnetically recoverable iron and a lower content of alkaline and sulfate impurities. These features make the magnetic fraction particularly attractive as a precursor for iron-based coagulants, while the silica-dominated non-magnetic fraction is well suited for utilization in ceramic formulations.

For completeness, the composition of the non-magnetic fraction was evaluated since it determines its suitability for downstream ceramic applications. SEM–EDS analysis shows that the non-magnetic fraction is silica-based, consisting primarily of Si and O, corresponding to approximately 90–95 wt.% SiO_2, with minor Al_2O_3 (~2–4 wt.%) and trace Fe-oxides (< 1 wt.%). XRD further confirms quartz and cristobalite as the dominant crystalline phases. This composition is characteristic of spent molding sands and refractory residues in casting operations and ensures reproducibility when incorporated into ceramic formulations, since SiO_2 serves as the primary skeletal phase, while low Fe content minimizes color contamination during firing.

3.2 Leaching of Iron from Iron-Containing Dust

The results of iron leaching from iron-containing dust are presented in Table 2. To quantify Fe^{2+} and Fe^{3+} species in the leachate, photocolorimetric measurements with sulfosalicylic acid complexation were performed. At pH 4–8, sulfosalicylic acid selectively complexes Fe^{3+} forming a red chelate ($\lambda = 500$ nm), while at pH 8–11.5 it complexes both Fe^{2+} and Fe^{3+} forming a yellow chelate ($\lambda = 425$ nm). Total Fe was determined at 425 nm, Fe^{3+} at 500 nm, and Fe^{2+} was calculated as the difference ($Fe^{2+} = Fe_{total} - Fe^{3+}$). Calibration curves ($R^2 > 0.998$) were constructed using analytical-grade $FeCl_3$ and Mohr's salt ($Fe(NH_4)_2(SO_4)_2 \cdot 6H_2O$) standards. Each measurement was performed in triplicate, and results are reported as mean values with a relative error of ± 10–15% depending on concentration.

As can be seen from Table 2, the maximum content of iron ions is achieved with a solid-to-liquid phase ratio of 1:7 (5:35). With a further increase in the volume of added hydrochloric acid, the concentration of Fe_{total} remains virtually unchanged, indicating the maximum possible extraction of iron from the waste under these conditions.

To establish the completeness of iron extraction from the waste, the elemental composition of the resulting sediment was determined after washing it to remove water-soluble compounds. The experimental results are presented in Table 3.

The elemental composition of the sediment indicates incomplete extraction of iron from the magnetic fraction of the ICD when treated with hydrochloric acid, even at a solid-to-liquid ratio of 1:7 or more. Therefore, the effect of suspension storage time on the extraction of iron ions from the waste was studied. For this, the experiment was carried out in the same way as before (5 g of the magnetic fraction of the ICD was treated with 35 mL

Table 2 Concentration of Fe^{2+}, Fe^{3+} and total Fe in the leachate after treating 5 g of the magnetic ICD fraction with different volumes of 18 wt% HCl

Volume of 18% hydrochloric acid, mL	Concentration, g/L		
	Fe^{3+}	Fe^{2+}	Fe_{total}
20	1.52	62.08	63.60
25	2.28	63.15	65.43
30	1.91	66.74	68.65
35	3.04	67.33	70.37
40	1.91	68.86	70.77
50	1.86	68.49	70.35

Table 3 SEM–EDS elemental composition of the solid residue obtained after treating the magnetic ICD fraction with different volumes of 18 wt.% HCl (wt.%)

Volume of 18% hydrochloric acid, mL	Elemental composition, wt.%			
	O	Si	Al	Fe
Initial	50.17	40.06	1.50	8.27
20	55.11	41.75	1.23	1.91
25	54.83	42.11	1.17	1.89
30	53.89	43.09	1.25	1.77
35	54.41	43.41	1.19	0.99
40	55.18	42.73	1.24	0.85
50	54.67	43.16	1.18	0.99

Table 4 Concentration of Fe^{2+}, Fe^{3+} and total Fe in the leachate after treating 5 g of the magnetic ICD fraction with 35 mL of 18 wt.% HCl and filtering after different storage times

Storage time, hours	Concentration, g/L		
	Fe^{3+}	Fe^{2+}	Fe_{total}
1	3.04	67.33	70.37
3	14.85	56.63	70.98
9	17.91	54.14	71.55
12	19.36	54.28	73.64
24	21.35	51.64	72.99
48	22.57	51.09	73.66

Table 5 SEM–EDS elemental composition of the solid residue obtained after filtration at different storage times (wt. %)

Storage time, hours	Concentration, g/L			
	O	Si	Al	Fe
1	54.41	43.41	1.19	0.99
3	55.13	42.97	1.19	0.71
9	54.27	44.16	1.24	0.33
12	53.11	45.67	1.22	-
24	54.97	43.86	1.17	-
48	53.86	44.91	1.23	-

of 18% hydrochloric acid and heated for 30 min at a temperature of 100 °C), but the cooling time was changed—from 1 h to 2 days (Table 4).

As can be seen from Table 4, with increasing storage time, the concentration of Fe_{total} and Fe^{3+} in the solution increases, with the most intense increase in the latter being observed, which is associated not only with an increase in iron extraction from the waste but also with the oxidation of Fe^{2+} to Fe^{3+}. The maximum concentration of Fe_{total} is reached after 12 h and then remains virtually unchanged. The complete extraction of iron from the magnetic fraction of the ICD after 12 h of storage is also evidenced by the elemental composition of the sediment obtained after filtration and washing from water-soluble salts (Table 5).

Figure 3 shows the XRD pattern (a) and SEM–EDS elemental distribution (b) of the sediment filtered after 12 h of storage. The XRD analysis confirms the absence of crystalline iron-bearing phases, indicating that iron was fully transferred into solution during the leaching stage. The dominant reflections correspond to silica phases (quartz and cristobalite), which are stable residues of the non-leached fraction. The SEM–EDS map further confirms the predominance of Si and O in the solid phase, while Fe signals remain below the detection threshold, corroborating the completeness of iron extraction under the applied leaching conditions.

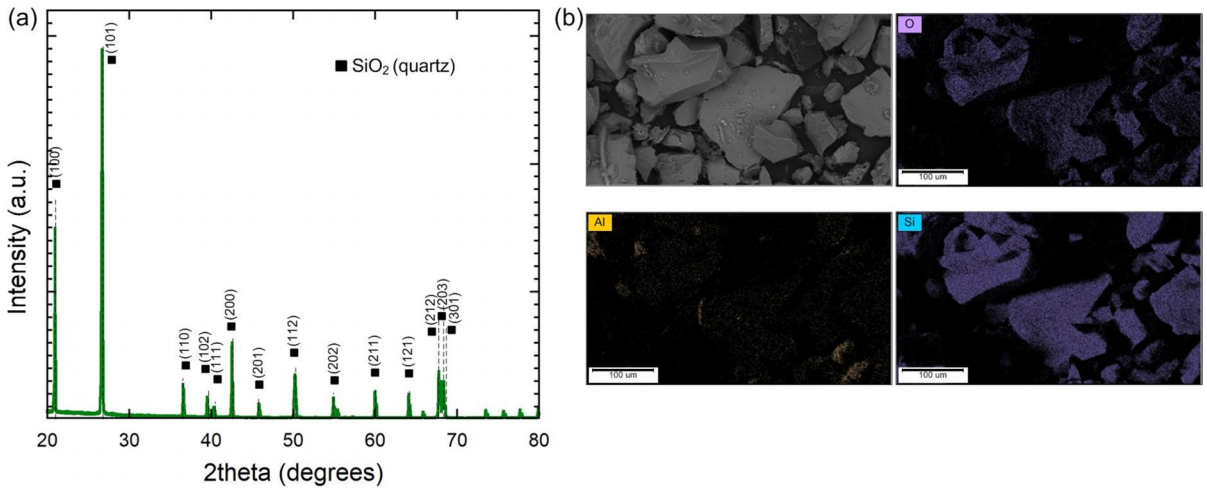

Fig. 3 XRD pattern **a** and SEM–EDS elemental analysis **b** of the solid residue obtained after 12 h storage and filtration of the leaching suspension

Based on the results of the experiments, the following conditions are proposed for the process of obtaining a solution of iron-containing coagulant from the magnetic fraction of iron-containing dust: i) use of the magnetic fraction of iron-containing dust; ii) ratio of the magnetic fraction and hydrochloric acid (18%) – 1:7 (7 mL of hydrochloric acid per 1 g of magnetic fraction); iii) heating for 30 min at a temperature of 100 ºC; iv) holding the suspension for 12 h; v) separation of the solid and liquid phases by filtration.

3.3 Determination of the Efficiency of a Coagulant Obtained from Iron-Containing Dust

The trial coagulation for WW1 from ceramic production was carried out at different pH values. The results of the experiment are shown in Fig. 4. It can be seen from Fig. 4 that a greater degree of purification is achieved in a neutral environment (pH 7).

The regression equation shows the dependence with high accuracy (Fig. 4b).

$$Ef = 43.8579 - 0.1114pH + 3.8035D - 0.6508pH^2 - 0.6733pHD - 0.1806D^2 + 0.2093pH^3 + 0.0843pH^2D - 0.0080pHD^2 + 0.0056D^3, R^2 = 0.9942$$

where pH is a pH, D is a dose of coagulant, mg/L.

During the test of coagulation of wastewater samples WW2 from glaze production and WW3 from a fermented milk production facility, it was found that at pH 5 and pH 6, there is virtually no purification from colloidal impurities. At pH 7, there is intense flocculation followed by rapid sedimentation of the flocs. Thus, it is advisable to carry out wastewater purification from suspended solids using the experimental coagulant in a neutral environment. The graph of the dependence of the purification efficiency of wastewater WW1-3 on the dose of the obtained iron-containing coagulant is shown in Fig. 5. All measurements were carried out at pH 7. The graph shows that the degree of purification increases with an increase in the coagulant dose up to a certain point, after which it practically does not change. Therefore, a further increase in the coagulant dose (above 37.5 mg of dry matter per 1 L of wastewater) did not make sense.

To study the sedimentation process of suspended matter over time, sedimentation kinetic curves were constructed. Each figure (Fig. 6 a, b c) shows three dependences of purification efficiency on time: i) for wastewater untreated with a coagulant; ii) for wastewater treated with an experimental coagulant; iii) for wastewater treated with the industrial coagulant $FeCl_3$.

In Fig. 6 a, b, c it is evident that the process of wastewater purification using the experimental coagulant does not differ from the process of wastewater purification using the industrial coagulant. However, to achieve the specified purification efficiency (about 97–98%) of all three model wastewaters using the experimental coagulant, its dose is many times less than the dose of the industrial coagulant (Fig. 7).

Thus, in the first two cases, the dose of the experimental coagulant is almost 6 times less than the dose of the industrial coagulant, and in the third case, it is almost 12 times less. This may be due to

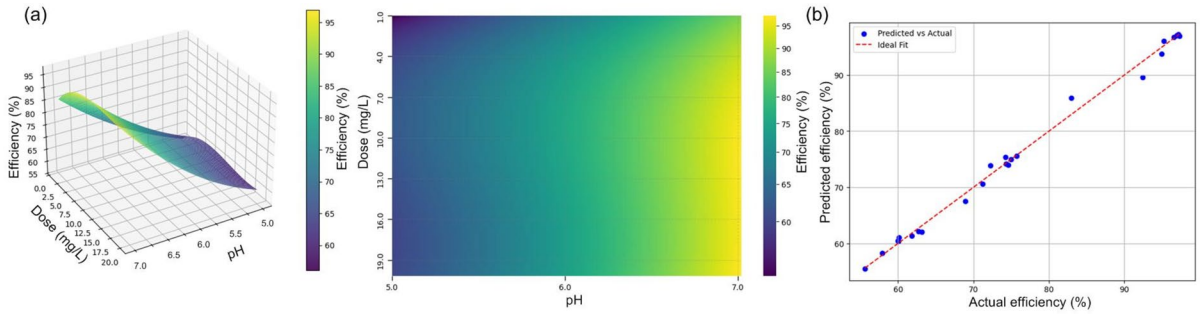

Fig. 4 Coagulation performance for model wastewater WW1 under different pH conditions **a**, and correlation between predicted and measured removal efficiencies **b**

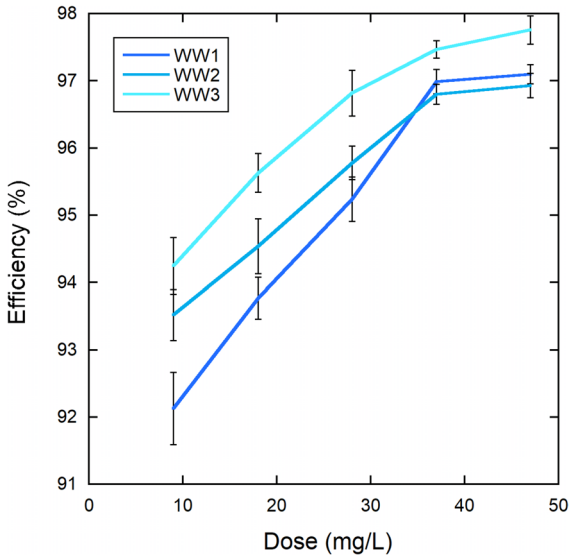

Fig. 5 Effect of coagulant dosage on purification efficiency for model wastewaters WW1–WW3 at pH 7 (SD between 3 replicates)

the formation of silicic acids during the treatment of iron-containing foundry dust with hydrochloric acid since it contains SiO_2. In this case, the process of polycondensation of silicic acids is possible, accompanied by the formation of polysilicic acids, which are good flocculants, as a result of which the resulting coagulant will also exhibit flocculating properties. This, in turn, contributes to the formation of large flakes, which intensifies the process of wastewater purification from fine and colloidal impurities. The performance of the synthesized iron-based coagulant can be explained by the well-known hydrolysis and precipitation behavior of Fe(III) salts in water (Prakash et al., 2014; Richardson & Connelly, 2018). Upon dissolution, Fe^{3+} hydrolyzes to form positively charged hydroxo-complexes and amorphous $Fe(OH)_3$, which destabilize negatively charged colloids via a combination of charge neutralization and sweep flocculation (Owodunni & Ismail, 2021; Prakash et al., 2014). The optimal removal observed at pH 5–7 corresponds to the maximum formation of polymeric Fe-hydroxides, whereas lower performance at acidic and alkaline pH reflects incomplete hydrolysis (<4) or the formation of negatively charged complexes (>8), consistent with reports for commercial ferric coagulants (Peters et al., 1987; Richardson & Connelly, 2018). This mechanistic behavior explains both the pH dependence and the lower dosage required compared to $FeCl_3$, as observed in our experiments. When placed in the context of recent studies on waste-derived iron coagulants, the performance of the ICD-based coagulant is comparable to or better than that reported for red-mud-based coagulants, coagulants obtained from acid mine drainage and spent pickling liquors, and iron-bearing industrial residues (Almeida & Schneider, 2020; Matei et al., 2022; Mwewa et al., 2019; Orescanin et al., 2002; Poulin et al., 2008). Many of these systems achieve similar clarification efficiencies, but often require higher dosages, multi-step synthesis or the use of additional oxidants and neutralization agents. In contrast, the coagulant synthesized from foundry dust in this work reaches

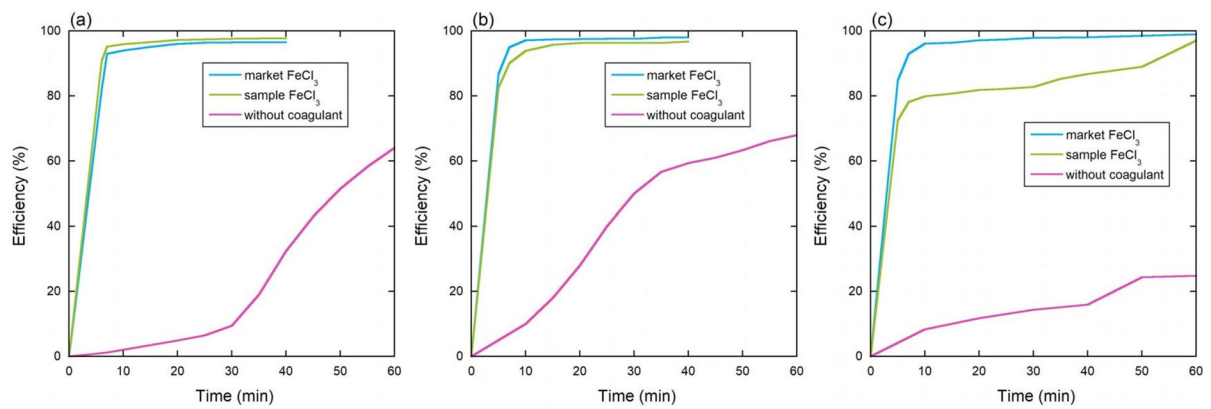

Fig. 6 Sedimentation kinetics of suspended solids in model wastewaters WW1 from ceramic production **a**, WW2 from glaze production **b**, WW3 from a fermented milk production facility **c** for untreated samples, samples treated with the experimental coagulant, and samples treated with commercial $FeCl_3$

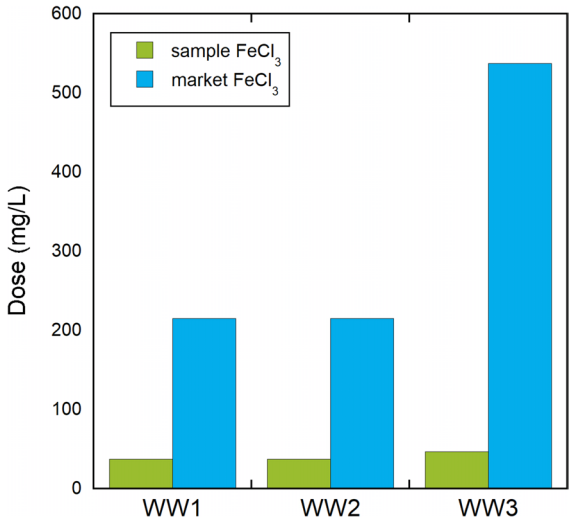

Fig. 7 Coagulant dosages required to achieve 97% removal efficiency in WW1 from ceramic production and WW2 from glaze production) and 98% (for WW3 from a fermented milk production facility)

95–98% removal at an optimal dose of 37.5 mg/L and 6–12 times lower dosage than commercial $FeCl_3$, using a relatively simple one-stage HCl leaching route. Furthermore, unlike most published approaches that focus solely on coagulant production, our process also enables the beneficial utilization of the silica-rich non-magnetic fraction in ceramic formulations, which enhances the circularity and practical attractiveness of the proposed technology (Matei et al., 2022; Zalyhina et al., 2022).

3.4 Technology for Obtaining Coagulant from Foundry ICD

The process flow chart of the iron-containing coagulant production process is shown in Fig. 8. Iron-containing dust is loaded into magnetic separator 1. The magnetic field forces attract iron-containing particles and separate them from the mixture. The non-magnetic fraction enters dosing bin 2, and the magnetic fraction enters dosing bin 3. Hydrochloric acid supplied by a third-party manufacturer does not always correspond to the required concentration. Therefore, a stage of preparing an acid solution of a given concentration is provided. Water from reservoir 5 is fed into the tank with mixer 4 in the volume required for dilution. Then, concentrated hydrochloric acid is dosed from reservoir 6. After separation, the magnetic fraction is dosed into reactor-mixer 7, which is equipped with a heating jacket. Then, it is treated with a solution of 18% hydrochloric acid. The heating jacket maintains a temperature of 100 ºC in the reactor. From the upper part of the reactor, gases and vapors enter condenser 8, where they condense, then separator 9. In the separator, condensate and uncondensed gas are separated. Condensate is returned to the reactor. Uncondensed gas, hydrogen, is discharged through a drip collector into the general exchange ventilation. After 30 min, after the process of vigorous hydrogen evolution is complete, the reaction mixture is maintained at room temperature for two days. After the maintenance, the suspension undergoes a filtration stage. The mixture is fed into the Nutsche filter 10. The sediment remains on the filter partition, and the filtrate exits through the branch pipe under the influence of the vacuum created by a vacuum pump. The resulting filtrate is the iron-containing coagulant. To wash the sediment, wash water is fed into Nutsche filter 10. The wastewater is discharged through the branch pipe under the influence of a vacuum. The wet sediment is placed in a drying oven 11. At a temperature of 100 ºC for 4 h, the sediment dries completely.

3.5 Use of Leaching Sludge and Non-Magnetic Fraction of Liquid-Coal-Bearing Minerals in the Production of Artistic Ceramics

The resulting sediment, as well as the non-magnetic fraction of the ICD, mainly consists of SiO_2 (Fig. 2), so it is proposed to use them in the production of ceramics, as was done in a number of articles (Ademati et al., 2022; Akinwande et al., 2023a, 2023b; Barnabas et al., 2023; Zalyhina et al., 2024). The paper investigated the use of the named waste in the production of artistic ceramics. The scheme of the research is presented in Fig. 9.

The obtained samples are shown in Fig. 10.

As experimental studies have shown, the density and water absorption of all samples are almost the same (density 1890–1910 kg/m^3, water absorption 11.7–12.1%). With an increase in the waste content, the shrinkage of products decreases slightly (from 13.5 to 11.8%), since the waste acts as a lean additive.

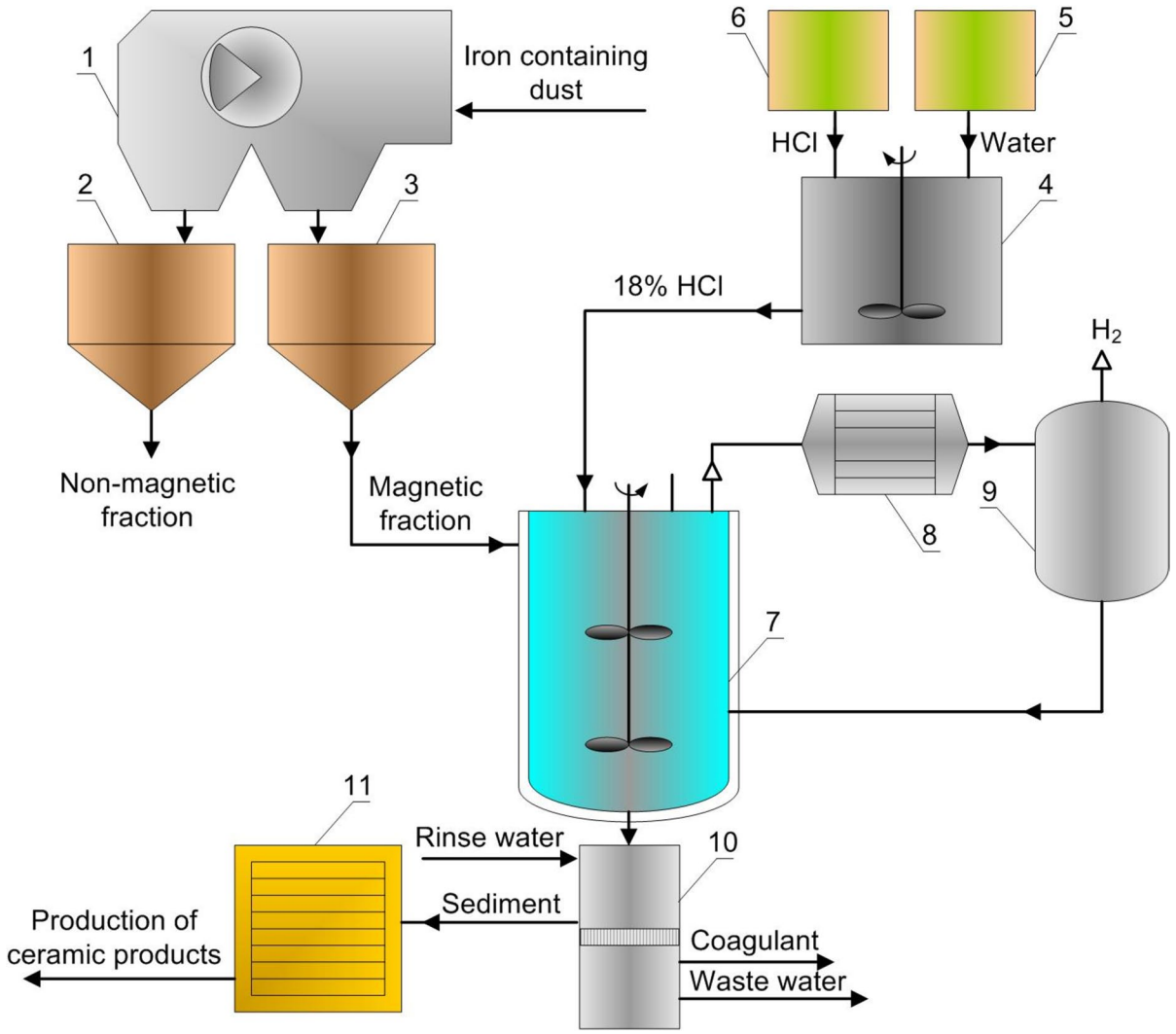

Fig. 8 Process flow diagram for producing iron-based coagulant from foundry dust: 1—magnetic separator; 2—dosing bin (non-magnetic fraction); 3 — dosing bin (magnetic fraction); 4—acid preparation tank; 5—water reservoir; 6—concentrated HCl reservoir; 7—reactor–mixer with heating jacket; 8—condenser; 9—gas–liquid separator; 10—Nutsche filter; 11—drying oven

A limitation of the present study is that the coagulation tests were performed on three model wastewater types under controlled laboratory conditions, and therefore do not fully capture the complexity of real industrial wastewater matrices with fluctuating pH, ionic strength, organic load and competing colloids. In addition, only short-term coagulation and settling behavior was evaluated, without assessing long-term sludge stability, dewatering behavior or potential release of bound metals. The economic and life-cycle implications of replacing commercial coagulants with foundry-waste-derived materials were not assessed and require future techno-economic and LCA studies. Finally, while the non-magnetic fraction was successfully utilized in ceramic products at laboratory scale, industrial-scale processing parameters, mechanical performance and leaching safety evaluations were beyond the scope of this work.

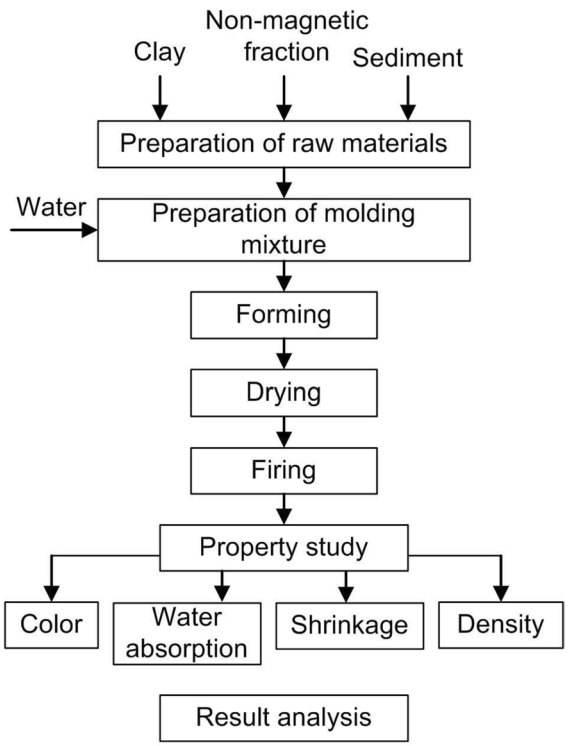

Fig. 9 Scheme for incorporating solid residues and non-magnetic fractions into ceramic products

4 Conclusion

In this study, iron-containing foundry dust was successfully converted into a functional iron-based coagulant capable of removing 95–98% of suspended and colloidal impurities at an optimal dose of 37.5 mg/L in the pH range 5–7, demonstrating performance comparable to commercial $FeCl_3$ but at 6–12 times lower dosage. This provides clear environmental and economic advantages by enabling the valorization of high-volume industrial waste and reducing chemical consumption during wastewater treatment. In addition, the non-magnetic fraction and leaching residues rich in SiO_2 were successfully incorporated into ceramic products, demonstrating the potential for near-zero-waste utilization and alignment with circular economy concepts. A practical roadmap for industrial scale-up includes: (i) validation of coagulant performance on real industrial wastewater streams with fluctuating matrix composition, (ii) engineering of continuous leaching and filtration units with corrosion-resistant materials, (iii) techno-economic and life-cycle assessments comparing waste-derived coagulants with commercial salts, and (iv) regulatory and product certification steps for both the coagulant and ceramic by-products. Overall, the proposed approach offers a feasible pathway for foundries and

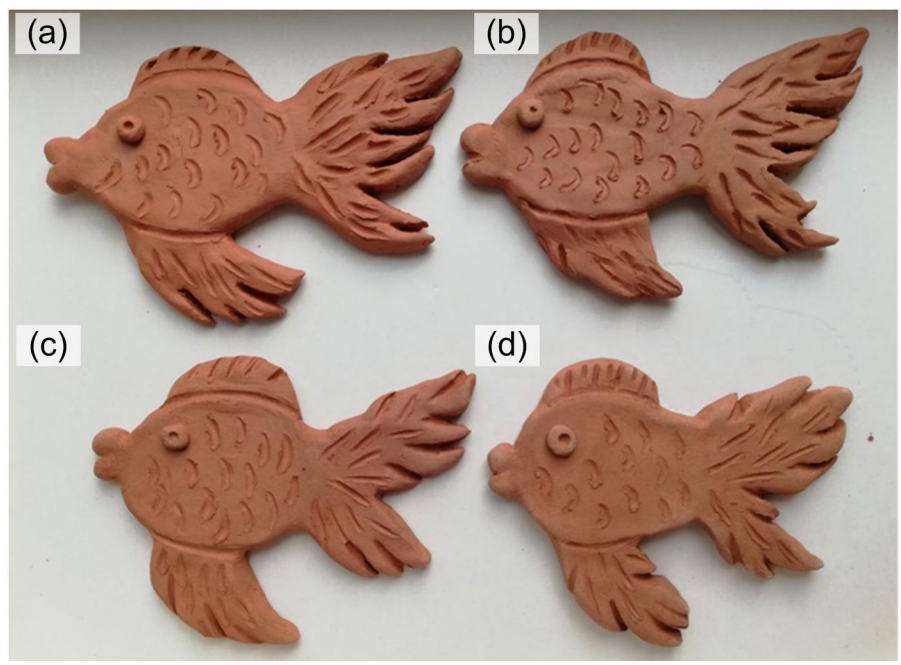

Fig. 10 Ceramic samples containing different amounts of solid waste: **a** 0 wt.%, **b** 10 wt.%, **c** 20 wt.%, and **d** 30 wt.%

water treatment facilities to reduce waste disposal costs, generate value-added products, and meet sustainability requirements, supporting large-scale industrial adoption.

Authors Contribution **Volha Zalyhina**: supervision, conceptualization, methodology, validation, investigation, formal analysis, data curation, visualization, writing – original draft. **Valentin Romanovski**: methodology, validation, investigation, formal analysis, data curation, visualization, writing – original draft, writing – review and editing.

Funding Not applicable.

Data Availability All data, models, and code generated or used during the study appear in the submitted article.

Declarations

Ethics Approval Not applicable.

Consent for Publication Not applicable.

Competing Interest The authors declare no competing interest with any previous work.

References

Ademati, A. O., Akinwande, A. A., Balogun, O. A., & Romanovski, V. (2022). Optimization of bamboo fiber–reinforced composite-clay bricks for development of low-cost farm settlements toward boosting rural agribusiness in Africa. *Journal of Materials in Civil Engineering, 34*(12), Article 04022335.

Akinwande, A. A., Balogun, O. A., Danso, H., Romanovski, V., Ademati, A. O., & Oyediran, A. O. (2023a). Development of insulating masonry bricks from wood fiber and varying milled glass proportion. *Journal of Civil Engineering and Construction, 12*(1), 40–54.

Akinwande, A. A., Folorunso, D. O., Balogun, O. A., Danso, H., & Romanovski, V. (2023b). Paperbricks produced from wastes: Modeling and optimization of compressive strength by response surface approach. *Environmental Science and Pollution Research, 30*(3), 8080–8097.

Almeida, V. O., & Schneider, I. A. (2020). Production of a ferric chloride coagulant by leaching an iron ore tailing. *Minerals Engineering, 156*, Article 106511.

Barnabas, A. A., Balogun, O. A., Akinwande, A. A., Ogbodo, J. F., Ademati, A. O., Dongo, E. I., & Romanovski, V. (2023). Reuse of walnut shell waste in the development of fired ceramic bricks. *Environmental Science and Pollution Research, 30*(5), 11823–11837.

Beletskii, E. V., & Romanovski, V. (2024). Direct plasma solution recycling of cathode materials for lithium-ion batteries with simultaneous removal of contaminants and relithiation. *Journal of Power Sources, 624*, Article 235576.

Blel, W., Dif, M., & Sire, O. (2015). Effect of a new regeneration process by adsorption-coagulation and flocculation on the physicochemical properties and the detergent efficiency of regenerated cleaning solutions. *Journal of Environmental Management, 155*, 1–10.

Bratchun, V. I., Bespalov, V. L., Ahmed Alani, A., Zhevanov, V. V., & Romasyuk, E. A. (2024). Hydraulic activity of crushing screenings of waste open-hearth slag. *Construction Materials and Products, 7*(3), 3. https://doi.org/10.58224/2618-7183-2024-7-3-3

Brigida, V., Golik, V., Voitovich, E., Kukartsev, V., Gozbenko, V., Konuhov, V., & Oparina, T. (2024). Technogenic reservoirs resources of mine methane when implementing the circular waste management concept. *Resources, 13*, 33. https://doi.org/10.3390/resources13020033

Couperthwaite, S. J., Johnstone, D. W., Millar, G. J., & Frost, R. L. (2013). Neutralization of acid sulfate solutions using bauxite refinery residues and its derivatives. *Industrial & Engineering Chemistry Research, 52*(4), 1388–1395.

Gruzinova, V., & Romanovski, V. (2025). Optimizing oil-contaminated wastewater purification with aluminum coagulants. *Water, Air, & Soil Pollution*. https://doi.org/10.1007/s11270-025-07928-w

Gudkov, A. G., Pavlov, M. V., Karpov, D. F. (2021). Mass transfer in a layer of aluminized glass-fiber material in the treatment of chrome-containing wastewater. IOP Conference Series: Materials Science and Engineering. 1079(5). 062041. https://iopscience.iop.org/article/https://doi.org/10.1088/1757-899X/1079/6/062041

Gudkov, A. G., Pavlov, M. V., Karpov, D. F. (2022). Hydrodynamic parameters when filtering chromium-containing wastewater through a layer of fibrous waste. IOP Conference Series:Earth and Environmental Science. 990. 012049. https://iopscience.iop.org/article/https://doi.org/10.1088/1755-1315/990/1/012049

Gurgenidze, D., & Romanovski, V. (2023). The pharmaceutical pollution of water resources using the example of the Kura River (Tbilisi, Georgia). *Water, 15*(14), Article 2574.

Kamarou, M., Tan, H., Moskovskikh, D., Kulinich, N., Ma, X., Yang, F., & Romanovski, V. (2025). High strength anhydrite cement based on lime mud from water treatment process: One step synthesis in water environment, characterization and technological parameters. *Engineering Reports, 7*(1), Article e13054.

Klyuev, S. V., Slobodchikova, N. A., Saidumov, M. S., Abumuslimov, A. S., Mezhidov, D. A., & Khezhev, T. A. (2024). Application of ash and slag waste from coal combustion in the construction of the earth bed of roads. *Construction Materials and Products, 7*(6), Article 3. https://doi.org/10.58224/2618-7183-2024-7-6-3

Kozlovskaya, I., Martsul, V., & Romanovski, V. (2024). Value-added Lanthanum-Containing Products Recovered from Spent Cracking Catalyst. *ACS Sustainable Resource Management, 1*(12), 2593–2601.

Lal, K., & Garg, A. (2019). Effectiveness of synthesized aluminum and iron based inorganic polymer coagulants for pulping wastewater treatment. *Journal of Environmental Chemical Engineering, 7*(5), Article 103204.

Ma, L., Ghorbani, Y., Kongar-Syuryun, C., Khairutdinov, M., Klyuev, R., Petenko, A., & Brigida, V. (2024). Dynamics of backfill compressive strength obtained from enrichment tails for the circular waste management. *Resources Conservation & Recycling Advances, 23*, Article 200224. https://doi.org/10.1016/j.rcradv.2024.200224

Malyukova, L., Martyushev, N., Tynchenko, V., Kondratiev, V., Bukhtoyarov, V., Konuhov, V., Bashmur, K., Panfilova, T., & Brigida, V. (2023). Circular mining wastes management for sustainable production of *Camellia sinensis* (L.) O. Kuntze. *Sustainability, 15*, Article 11671. https://doi.org/10.3390/su151511671

Martsul, V. N., Zalygina, O. S., Likhacheva, A. V., & Romanovski, V. I. (2013). Treatment of electroplating shop wastewater at enterprises of the Republic of Belarus. Proceedings of BSTU. *Chemistry and Technology of Inorganic Substances 3*, 57–62.

Matei, E., Predescu, A. M., Păulean, A. A., Râpă, M., Sohaciu, M. G., Coman, G., & Vlad, G. (2022). Ferrous industrial wastes—valuable resources for water and wastewater decontamination. *International Journal of Environmental Research and Public Health, 19*(21), Article 13951.

Matsukevich, I. V., Beljin, J., Kulinich, N. V., Apostolović, T., Maletić, S., & Romanovski, V. (2025). Photocatalytic degradation of polycyclic aromatic hydrocarbons under visible light irradiation in water using TiO2/MgO nanocomposites. *Environmental Science and Pollution Research*. https://doi.org/10.1007/s11356-025-36055-6

Mwewa, B., Stopić, S., Ndlovu, S., Simate, G. S., Xakalashe, B., & Friedrich, B. (2019). Synthesis of poly-alumino-ferric sulphate coagulant from acid mine drainage by precipitation. *Metals, 9*(11), 1166.

Orescanin, V., Tibljas, D., & Valkovic, V. (2002). A study of coagulant production from red mud and its use for heavy metals removal. *Journal of Trace and Microprobe Techniques, 20*(2), 233–245.

Owodunni, A. A., & Ismail, S. (2021). Revolutionary technique for sustainable plant-based green coagulants in industrial wastewater treatment—A review. *Journal of Water Process Engineering, 42*, Article 102096.

Peters, R. W., Oresik, W. L., Engelder, C. L., Gopalratnam, V. C., & Greenfield, J. (1987). Physical and chemical methods. *Journal (Water Pollution Control Federation), 59*(6), 364–388.

Poulin, É., Blais, J. F., & Mercier, G. (2008). Transformation of red mud from aluminium industry into a coagulant for wastewater treatment. *Hydrometallurgy, 92*(1–2), 16–25.

Prakash, N. B., Sockan, V., & Jayakaran, P. (2014). Waste water treatment by coagulation and flocculation. *International Journal of Engineering Science and Innovative Technology, 3*(2), 479–484.

Richardson, P. F., & Connelly, L. J. (2018). Industrial coagulants and flocculants. In *Reagents in mineral technology* (pp. 519–558). Routledge. https://doi.org/10.1201/9780203741214

Romanovski, V., Pilipenko, M., Dubina, A., Likhavitski, V., Volodko, S., Moskovskikh, D., & Romanovskaia, E. (2025). Optimizing dye wastewater purification: Ultrasonic and flotation with ozonation synergy. *Engineering Reports, 7*(1), Article e13044.

Romanovski, V., Dubina, A., Sehat, A. A., Su, X., & Moskovskikh, D. (2024). Green and bio-waste-based materials for energy production, conversion, storage, and hybrid technologies. In *Materials for energy production, conversion, and storage* (pp. 118–135). CRC Press. https://doi.org/10.1201/9781003318859-8

Romanovskiy, V. I. (2011). Thermochemical and mechanochemical treatment of used-up synthetic ionites producting valuable chemicals and sorption materials. *Science Prospects, 4*, 19.

Stevenson, R. A., Beard, P. J., & Banks, H. O. (1933). Chemical sewage purification at palo alto. Regeneration of spent coagulant effects complete sewage treatment. *Sewage Works Journal, 5*(1), 53–60.

Tuzhilin, A. S., Balmaev, B. G., & Vetchinkina, T. N. (2020). Comparative technical-and-economical evaluation of production costs of coagulant from technical-grade aluminum hydroxide and hydroxide sluge. In *IV Congress "Fundamental Research and Applied Developing of Recycling and Utilization Processes of Technogenic Formations" (TECHNOGEN 2019)* (pp. 344–349). Knowledge E. Ekaterinburg.

Vafaeva, K. M., Murtazaliev, M., & Demirci, N. (2024). Sustainable Digital. *Waste Management., 1*, 10–14. https://doi.org/10.5281/zenodo.14580438

Yelaman, A.; Alzhanova, G.; Iskakova, Z.; Abdiyussupov, G.; Omirzak, M.; Gazizova, A.; Vafaeva, K.M. (2025). Optimization of road-building materials from industrial waste (red mud, blast furnace slag, lime production waste, and natural loams). Frontiers in Materials. 11. https://doi.org/10.3389/fmats.2024.1400935.

Zalyhina, V., Cheprasova, V., & Romanovski, V. (2021). Pigments from spent ammonium chloride zinc plating electrolytes. *Journal of Chemical Technology & Biotechnology, 96*(10), 2767–2774.

Zalyhina, V., Cheprasova, V., & Romanovski, V. (2022). Paper industry slag for the production of building ceramics. *Journal of Chemical Technology & Biotechnology, 97*(11), 3091–3099.

Zalyhina, V., Cheprasova, V., & Romanovski, V. (2024). Recycling of fine fraction of spent foundry sands into fireclay bricks. *Journal of Material Cycles and Waste Management, 26*(1), 322–330.

Zhao, Y., Zhang, L. Y., Ni, F., Xi, B., Xia, X., Peng, X., & Luan, Z. (2011). Evaluation of a novel composite inorganic coagulant prepared by red mud for phosphate removal. *Desalination, 273*(2–3), 414–420.